

Structure–Property Relationship in Biodegradable Poly(butylene succinate)/Layered Silicate Nanocomposites

Suprakas Sinha Ray,[†] Kazuaki Okamoto,[‡] and Masami Okamoto^{*,†}

Advanced Polymeric Materials Engineering, Graduate School of Engineering, Toyota Technological Institute, Hisakata 2-12-1, Tempaku, Nagoya 468 8511, Japan, and Nagoya Municipal Research Institute, Rokuban 3-4-41, Atsuta, Nagoya 456-0058, Japan

Received December 2, 2002

ABSTRACT: Understanding the structure–property relationship in polymer/layered silicate nanocomposites is of fundamental importance in designing materials with desired properties. To understand these relations in the case of poly(butylene succinate) (PBS)/organically modified layered silicate (OMLS) nanocomposites, we studied the rheological properties of these materials in detail, because the rheological behavior of polymer/OMLS nanocomposites is strongly influenced by their nanostructure and the interfacial characteristics. For this reason, a series of PBS/OMLS nanocomposites were prepared using a simple melt intercalation technique. Two different types of OMLS, montmorillonite (mmt) modified with octadecylammonium chloride and saponite (sap) modified with quaternary hexadecyl tri-*n*-butylphosphonium bromide, were used for the nanocomposite preparations. The structure of nanocomposites in the nanometer scale was characterized using wide-angle X-ray diffraction (WAXD) analyses and transmission electron microscopy (TEM) observations. A flocculated structure has a strong effect on mechanical properties (both in solid and melts) and various other materials properties.

Introduction

Recently, polymer/layered silicate nanocomposites have attracted great interest from researchers, both in industry and in academia, because they often exhibit remarkable improvement of materials properties when compared with those for pure polymer or conventional composites (both micro- and macrocomposites). These improvements can include high moduli,¹ increased strength and heat resistance,² decreased gas permeability³ and flammability,⁴ and increased biodegradability of biodegradable polymers.⁵ On the other hand, these materials have also been proven to be unique model systems to study the structure and dynamics of polymers in confined environments.⁶

The main reason for these improved properties in nanocomposites is interfacial interaction between matrix and OMLS as opposed to conventional composites. Layered silicates have layer thicknesses on the order of 1 nm and very high aspect ratios (e.g., 10–1000). A few weight percent of OMLS that are properly dispersed throughout the matrix thus create a much higher surface area for polymer–filler interfacial interactions than do conventional composites.⁷ On the basis of the strength of the polymer/OMLS interactions, structurally three different types of nanocomposites are achievable (Figure 1): *intercalated nanocomposites*, where insertion of polymer chains into the layered silicate structure occurs in a crystallographically regular fashion, regardless of polymer to OMLS ratio, and a repeat distance of few nanometer; *flocculated nanocomposites*, where intercalated stacked silicate layers some time flocculated due to the hydroxylated edge-edge interactions, and *exfoliated nanocomposites*, where the individual silicate

layers are separated in polymer matrix by average distances that totally depend on the clay loading.

Today, the development of biodegradable polymeric materials with excellent materials properties is a subject of active research interest worldwide. Aliphatic polyesters are among the most promising materials for the production of high performance environment friendly biodegradable plastics.⁸ Biodegradation of aliphatic polyester is well-known, in that some living organisms degrade them by producing enzymes, which attack the polymer.⁹ One of them is poly(butylene succinate) (PBS, Scheme 1) with the trade name “BIONOLLE”, and it is chemically synthesized by polycondensation of 1,4-butanediol with succinic acid. PBS is a commercially available, aliphatic thermoplastic polyester with many interesting properties, including biodegradability, melt processability, and thermal and chemical resistance.¹⁰ PBS has excellent processability, so it can be processed in the field of textiles into melt blow, multifilament, monofilament, nonwoven, flat, and split yarn and also in the field of plastics into injection-molded products,¹¹ thus being a promising polymer for various potential applications. However, other properties of PBS, such as softness, gas barrier properties, and melt viscosity for further processing etc. are often not sufficient for various end-use applications.

In a natural extension of our ongoing research on biodegradable polylactide (PLA)/OMLS nanocomposites (PLACNs),^{5,12–15} we have applied this nanocomposite technology to PBS in order to get material with improved materials properties suitable for wide range of applications. In our previous paper,¹⁶ we have reported on the preparation and characterization of intercalated PBS/montmorillonite (mmt) nanocomposites. In this paper, we report details of the structural characterization and rheological behavior of a series of PBS/OMLS nanocomposites because the measurement of rheological properties of polymeric materials is crucial to gain a fundamental understanding of the structure–property

* To whom correspondence should be addressed. Telephone: +81-52-809 1861. Fax: +81-52-809 1864. E-mail: okamoto@toyota-ti.ac.jp.

[†] Toyota Technological Institute.

[‡] Nagoya Municipal Research Institute.

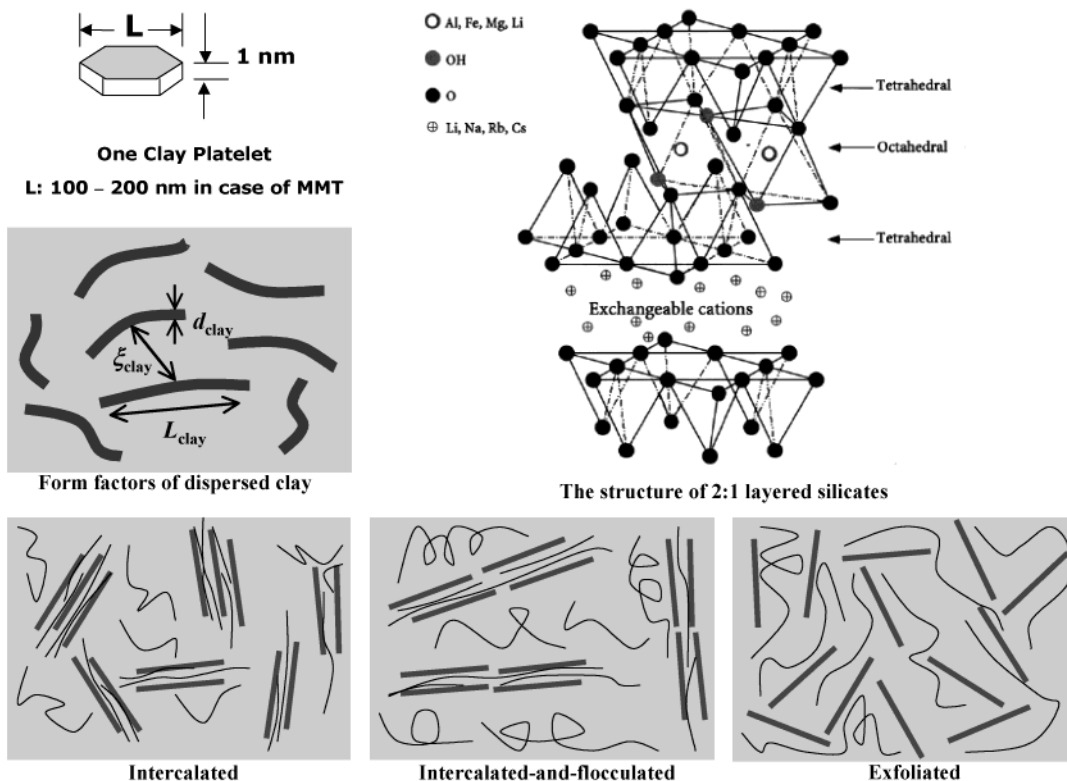
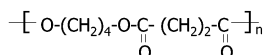
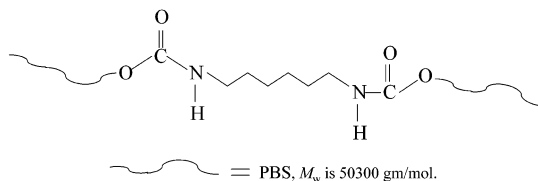


Figure 1. Schematic illustration of three broad classes of thermodynamically achievable polymer/layered silicate nanocomposites.

Scheme 1. Structure of PBS



Scheme 2. Formation of Urethane Bonds in High Molecular Weight PBS



relationship and also the nature of processability for these materials. Aside from these on the basis of viscoelastic behavior under molten state we can easily find out the strength of polymer/OMLS interactions in the case of PBSCNs. Finally, we show some of our preliminary results on the biodegradability of neat PBS and nanocomposites.

Experimental Section

Materials. PBS (PBS#1020) used in this study is a commercial product of Showa Denko Co. and was dried in an airflow oven prior to use. High molecular weight PBS used in this research was prepared by a coupling reaction of relatively low molecular weight PBS in the presence of hexamethylene diisocyanate ($\text{OCN}-\text{C}_6\text{H}_{12}-\text{NCO}$) as a chain extender. For example, 4.07 kg of hexamethylene diisocyanate was added to the reactor containing 339 kg of PBS (M_n and M_w are 18600 and 50 300 g/mol respectively) to perform a coupling reaction for 1 h at 180–200 °C. Each PBS chain has 0.48 wt % of chain extender and this group makes urethane type bonds (see Scheme 2) with hydroxy-terminated PBS having low molecular weight.¹⁷

OMLS were synthesized by replacing Na^+ in two different layered silicates with alkylammonium or alkylphosphonium cation by ion exchange. In Table 1, we presented detail

specifications and designations (as written in the text) of two different types of OMLS used in this research.

Nanocomposite Preparation. For nanocomposites preparation, the OMLS and PBS were first dry-mixed by shaking them in a bag. The mixture was then melt-extruded using a twin-screw extruder (KZW15-30TGN, Technovel Corp.) operated at 150 °C to yield nanocomposite strands. The color of the strands (light gray color when prepared with C_{18} -mmt but almost same color of PBS when prepared with qC_{16} -sap) depends on the color of used OMLS. Hereafter, nanocomposites were abbreviated as PBSCNs. The compositions of prepared PBSCNs are presented in Table 2. The strands were pelletized and dried under vacuum at 75 °C for 7 h to remove water. Dried PBSCNs pellets were then converted into sheets with a thickness of 0.7 to 1.5 mm with a minimal compressive pressure (for the preparation of bubble-free PBSCNs sheets) at 135 °C for 3 min using a hot press. The molded sheets were then quickly quenched between glass plates and then annealed at 60 °C for 1.5 h to crystallize isothermally before being subjected to various characterizations (except for melt-rheological measurements). The content of inorganic parts in each PBSCN was determined by burning the thick sample sheets at 950 °C in a furnace.

Characterization Methods. WAXD. WAXD experiments were performed for two different types of OMLS powders, neat PBS, and various PBSCNs, respectively, using a Maxlabo X-ray diffractometer (MAC Science Co., 3 kW, graphite monochromator, $\text{Cu K}\alpha$ radiation (wavelength, $\lambda = 0.154$ nm)), operated at 40 kV/20 mA. The samples were scanned in FT mode with a counting time of 2 s under the diffraction angle 2θ in the range 1–70°.

TEM. The nanoscale structures of various PBSCNs were investigated by means of a high-resolution TEM (H-7100, Hitachi Co.), operated at an accelerating voltage of 100 kV. The ultrathin sections (the edge of the sample sheets) with a thickness of 100 nm were microtomed at –80 °C using a Reichert Ultracut cryo-ultramicrotome without staining. The direction of the compression mold relative to the TEM samples surface was perpendicular.

Gel Permeation Chromatography (GPC). The number-average (M_n) and weight-average (M_w) molecular weights of

Table 1. Detail Specifications and Designation of OMLS Used in This Research

OMLS codes	pristine layered silicate (LS)	CEC (mequiv/100 g)	length (nm)	salts used for the modification of LS	suppliers
C ₁₈ -mmt	montmorillonite	110	~150	octadecylammonium cation	Nanacor Inc.
qC ₁₆ -sap	saponite	86.6	~55	quaternary hexadecyl tri <i>n</i> -butylphosphonium	CO-OP Chemicals Ltd.

Table 2. Composition and Characteristic Parameters of PBSCNs Based on PBS and Two Different Types of Organically Modified Layered Silicates

samples	type of OMLS	composition, wt %		$M_w \times 10^{-3}$ (g/mol)	M_w/M_n
		PBS	OMLS ^a		
PBS		100		103	4.0
PBSCN1	C ₁₈ -mmt	98.5	1.5 [1.07]	100	3.8
PBSCN2	C ₁₈ -mmt	97.5	2.5 [1.73]	99	3.6
PBSCN3	C ₁₈ -mmt	96.0	4.0 [2.80]	97	4.3
PBSCN4	C ₁₈ -mmt	94.5	5.5 [3.60]	100	4.5
PBSCN5	qC ₁₆ -sap	98.5	1.5 [1.04]	98	3.9
PBSCN6	qC ₁₆ -sap	94.5	5.5 [3.84]	98	3.8

^a Value in brackets indicates the percentage of the inorganic part measured after burning.

PBS matrix (before and after nanocomposites preparation) were determined by means of GPC (Tosoh HLC-8121), using polystyrene standards for calibration and chloroform as a carrier solvent at 40 °C with the flow rate of 0.5 mL/min. The results of GPC measurements are summarized in Table 2. From Table 2, GPC data clearly indicate that there is almost no degradation of PBS matrix after nanocomposites preparation with two different types of OMLS.

Dynamic Mechanical Analysis (DMA). Dynamic mechanical properties of neat PBS and various PBSCNs were measured using a Reometrics dynamic analyzer (RDAII) in the tension-torsion mode. The temperature dependence of dynamic storage modulus (G') and loss modulus (G'') and their ratio, $\tan \delta$, were conducted at a constant frequency (ω) of 6.28 rad·s⁻¹, a strain amplitude of 0.05% and in the temperature range -50 to +110 °C with a heating rate of 2 °C/min. The size of the test samples was 12 × 29 × 0.7 mm³.

Melt Rheology. Melt rheological measurements were also conducted on a RDAII instrument with a torque transducer capable of measurements over the range of 0.2–200 g·cm. Dynamic oscillatory shear measurements were performed by applying a time dependent strain of $\gamma(t) = \gamma_0 \sin(\omega t)$ and the resultant shear stress is $\sigma(t) = \gamma_0 [G' \sin(\omega t) + G'' \cos(\omega t)]$, with G' and G'' being the storage and loss modulus, respectively. Measurements were conducted by using a set of 25 mm diameter parallel plates with a sample thickness of ~1.5 mm and in the temperature range 120–150 °C. The strain amplitude was fixed to 5% to obtain reasonable signal intensities even at elevated temperature or low ω to avoid the nonlinear response. For each PBSCN investigated, the limits of linear viscoelasticity were determined by performing strain sweeps at a series of fixed ω 's. The master curves were generated using the principle of time-temperature superposition and shifted to a common reference temperature (T_{ref}) of 120 °C, which was chosen as the most representative of a typical processing temperature of PBS.

Steady-shear viscosity measurements were conducted at 120 °C using 25 mm diameter cone and plate geometry with cone angle of 0.1 rad. The steady-shear viscosity data reported in this paper were obtained as a function of both shear rate and time under different shear rates.

Measurement of O₂ Gas Transmission Rate. Oxygen gas transmission rate of neat PBS and various PBSCNs were measured at 20 °C and 90% relative humidity by the ASTM D-1434 differential pressure method (GTR-30XAU, Yanaco Co.). Test samples were prepared by compression molding (thickness ~ 300 μm), and melt-quenched samples were used for this measurement.

Biodegradability. The biodegradability of neat PBS, PBSCN4, and PBSCN6 was studied on a homemade compost instrument at 58 ± 2 °C. The compost used was prepared from

mixture of soybean dust (byproduct of tofu) and effective microorganisms (EM-germ; purchased from Meikin CO-OP). Before use, this mixture was sealed and fermented for 20 days at open-air temperatures. For this test, the sample sheets (prepared by compress molding with a thickness of 0.3 ± 0.02 mm) were first clipped with a 35 mm slide holder and then put into the compost. After 35 days, samples were recovered from the compost, rinsed with distilled water, and finally washed with methanol using an ultrasonic bath for 5 min.

Results and Discussion

Nanocomposite Structure. The nanocomposite structure has typically been elucidated using WAXD and TEM. WAXD offers a convenient method to determine the interlayer spacing of the clay layers in the original clay and in the intercalated polymer/clay nanocomposites. On the other hand, TEM allows a qualitative understanding of the internal structure through direct visualization. WAXD patterns for the pure C₁₈-mmt powder and various representative PBSCNs are presented in Figure 2a. The mean interlayer spacing of the (001) plane ($d_{(001)}$) for the C₁₈-mmt solid obtained by WAXD measurements is 2.31 nm ($2\theta \cong 3.82^\circ$) (Figure 2a). The pattern of PBS matrix (Figure 2b) is displayed here as a baseline to compare the existence of diffraction peaks coming from dispersed clay layers in the PBS matrix. In the case of PBSCN1, a very small peak is observed at $2\theta \cong 2.75^\circ$ ($\cong 3.2$ nm), corresponding to the (001) plane of the dispersed silicate layers in the PBS matrix. With increasing clay content, this peak becomes stronger and gradually shifted toward the higher diffraction angle at $2\theta \cong 3.16^\circ$ ($\cong 2.80$ nm) for PBSCN4, accompanied by the appearance of small peak. After calculation, it was confirmed that this reflection is due to (002) plane ($d_{(002)}$) of C₁₈-mmt (Figure 2a) dispersed in the PBS matrix. The difference in interlayer spacing between pure C₁₈-mmt powder and PBSCN1 to PBSCN4 after melt mixing is presumably due to the intercalation of PBS chains into the silicate galleries and coherent order of the silicate layers is much higher with increasing clay content. Note that the existence of sharp Bragg peak in PBSCNs after melt extrusion clearly indicates that the dispersed silicate layers still retain an ordered structure after melt extrusion.

Figure 2b represents WAXD patterns for pure qC₁₆-sap clay powder, neat PBS, and the corresponding PBSCNs, respectively. The interlayer gallery height, calculated as the difference of the $d_{(001)}$ distance obtained by WAXD and the individual layer thickness (~1 nm), for the pure qC₁₆-sap powder is ~1.88 nm ($2\theta \cong 4.69^\circ$). WAXD profile of PBSCN5 shows a nearly exfoliate structure of the dispersed silicate layers in PBS matrix but in the case of PBSCN6 with 3.84 wt % clay content it indicates a disordered intercalated structure with a (001) plane peak at $2\theta \cong 4.18^\circ$ ($\cong 2.14$ nm).

From WAXD patterns, the crystallite size of intercalated stacked silicate layers of each PBSCN is calculated by using Scherrer equation¹⁸ i.e., D is given by

$$D = \frac{k\lambda}{\beta \cos \Theta} \quad (1)$$

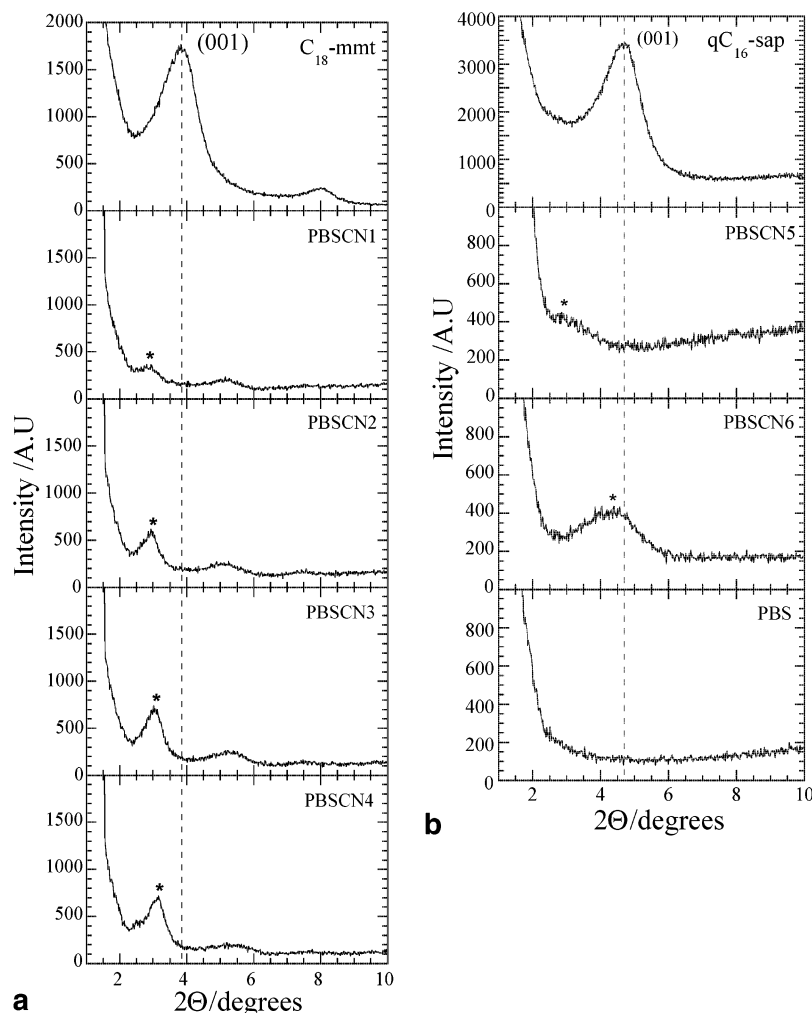


Figure 2. (a) WAXD patterns for pure C_{18} -mmt powder and corresponding PBSCNs. The dashed line indicates the location of the silicate (001) reflection of C_{18} -mmt. The asterisks indicate (001) peak for C_{18} -mmt dispersed in PBS matrix. (b) WAXD patterns for pure qC_{16} -mmt powder and corresponding PBSCNs. The dashed line indicates the location of the silicate (001) reflection of qC_{16} -sap. The asterisks indicate (001) peak for qC_{16} -mmt dispersed in PBS matrix.

Table 3. Form Factors of Various PBSCNs Obtained from WAXD Analyses and TEM Observations

	PBSCN1	PBSCN2	PBSCN3	PBSCN4	PBSCN5	PBSCN6
vol fraction of clay, ϕ_{clay}	0.004	0.007	0.011	0.014	0.004	0.015
WAXD						
d_{001}/nm	3.2	3.08	2.85	2.8		2.14
Δd_{001}^a	0.89	0.77	0.54	0.49	nearly exfoliate	0.27
D/nm^b	9.1	11.4	13.3	15.3	2–3	7.2
D/d_{001}	2.85	3.70	4.67	5.56		3.36
TEM						
$L_{\text{clay}}/\text{nm}$	339 ± 11	451 ± 14	715 ± 41	1721 ± 15	97 ± 17	367 ± 13
$\xi_{\text{clay}}/\text{nm}$	195 ± 55	117 ± 29	82 ± 35	69 ± 29	74 ± 21	54 ± 43
$L_{\text{clay}}/d_{\text{clay}}$	36–38	38–41	50–56	111–113	35–40	49–52

^a Δd_{001} is the extent of intercalation and can be define as $\Delta d_{001} = (d_{\text{PBSCN}} - d_{\text{OMLS}})$ nm. ^b Calculated from the Scherrer equation.¹⁸

where k is a constant (the value generally = 0.9), λ is the X-ray wavelength (= 0.154 nm), β is the width of the WAXD peak (in radian unit) and is measured by the full width at half-maximum, and θ is the WAXD peak position. The calculated value of D for each PBSCN is presented in Table 3.

The internal structure of the nanocomposites in the nanometer scale was directly observed via TEM analyses. Parts a–h of Figure 3 show the results of TEM bright field images of various PBSCNs corresponding to the WAXD experiments as shown respectively in parts a and b of Figure 2, in which dark entities are the cross section of intercalated organoclay layers.^{19,20}

The figures show both larger view, showing the dispersion of the clay within the PBS matrix, and a higher magnification, permitting the observation of discrete clay layers. For PBSCN1 (Figure 3, parts a and b), one can see that clay layers are stacked and flocculated, and an intercalated structure has been produced. In the case of PBSCN3 (Figure 3, parts c and d), we observe random orientation of the clay particles to the matrix surface, which consists of several stacked silicate layers. Actually, there is a large anisotropy of the stacked silicate layers. The size of the some of the stacked-silicate layers appears to reach about 600–700 nm in lengths. However, we cannot estimate the thick-

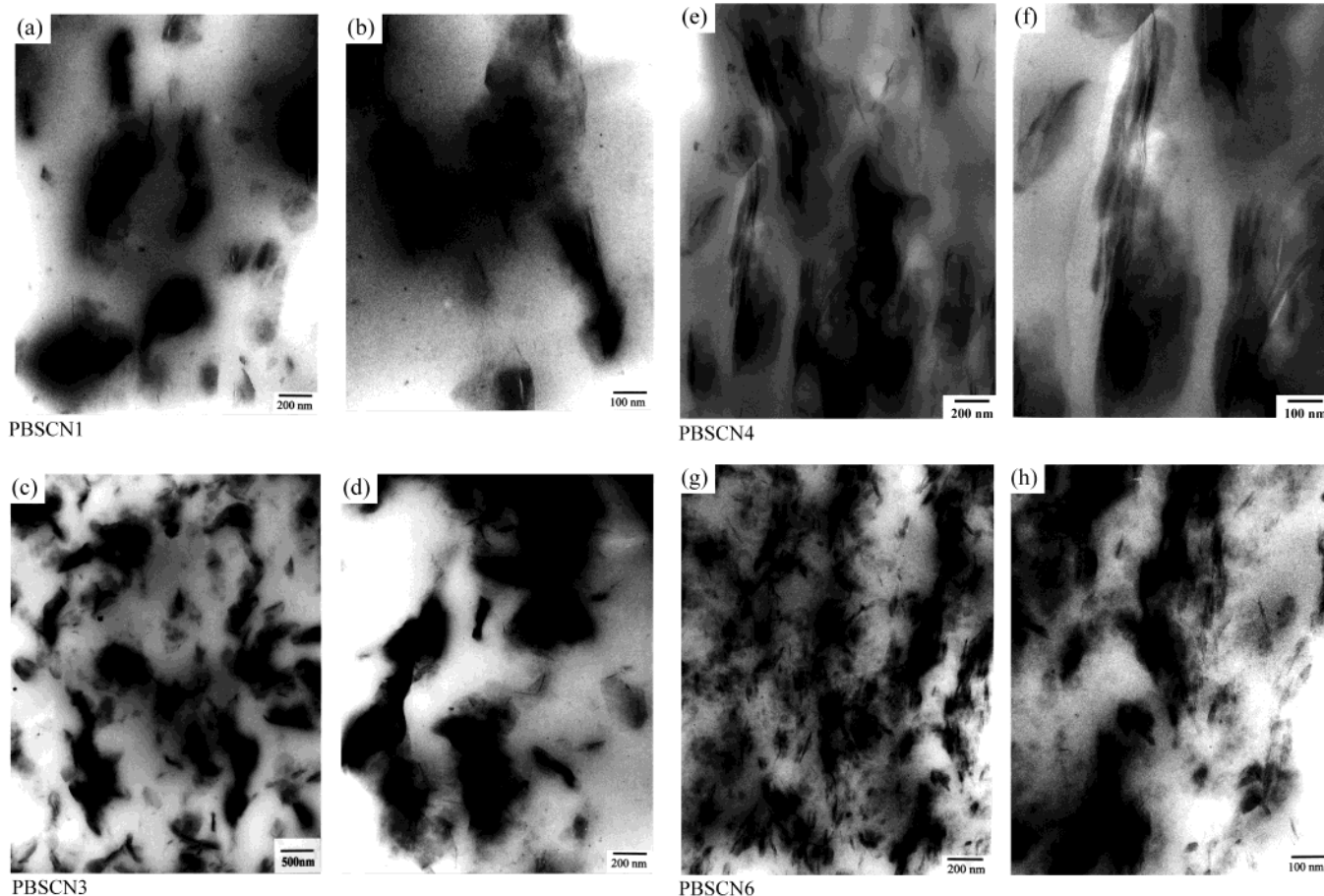


Figure 3. TEM bright field images of PBSCNs: (a) PBSCN1 ($\times 100000$), (b) PBSCN1 ($\times 200000$), (c) PBSCN3 ($\times 40000$), (d) PBSCN3 ($\times 100000$), (e) PBSCN4 ($\times 100000$), (f) PBSCN4 ($\times 200000$), (g) PBSCN6 ($\times 100000$), and (h) PBSCN6 ($\times 200000$) in which dark entities are the cross section of the intercalated or exfoliated silicate layers.

ness precisely from the TEM images. On the other hand, a well intercalated with strong flocculation structure is clearly observed with PBSCN4 (Figure 3, parts e and f).

At the other extreme, the TEM images of PBSCN6 (Figure 3, parts g and h) show fine and almost uniform distribution of clay particles in the PBS matrix where the clay particles exhibit both perpendicular and planar alignment to the sample surface. From the TEM images, it becomes clear that there are intercalated and disordered stacks silicate layers coexisting in the PBSCN6 structure. The intercalated structures are characterized by a parallel stacking that gives rise to the XRD reflection of PBSCN6 in Figure 2b, whereas the disordered clay formations have no periodic stacking and thus remain XRD silent.

In Table 3, we summarized the form factors (Figure 1) obtained from WAXD analyses and TEM observations i.e., average length (L_{clay}) and thickness ($D \equiv d_{\text{clay}}$) of the dispersed intercalated silicate layers, and the correlation length (ξ_{clay}) between them. Thus, on the basis of WAXD analyses and TEM observations, we can conclude that PBSCNs prepared using C₁₈-mmt clay clearly indicates the formation of ordered intercalated nanocomposites with flocculated structure and coherence order of the silicate layers gradually increases with increasing OMLS content, while those prepared with qC₁₆-sap clay leads to the formation of either near to exfoliate or disordered intercalated nanocomposites depending on the amount of clay loading.

Solid-State Rheology and Enhancement of Modulus. Dynamic mechanical analysis (DMA) measures the response of a given material to an oscillatory deformation (here in tension-torsion mode) as a function of temperature. DMA results are expressed by three main parameters: (a) the storage modulus (G') corresponding to the elastic response to the deformation, (b) the loss modulus (G''), corresponding to the plastic response to the deformation, and (c) $\tan \delta$, that is the (G''/G') ratio, useful for determining the occurrence of molecular mobility transitions such as the glass transition temperature (T_g).

Here DMA analysis has been studied to track the temperature dependence of G' , G'' , and $\tan \delta$ of neat PBS upon PBSCNs formation with two different types of OMLS. Parts a and b of Figure 4 show the temperature dependence of G' , G'' , and $\tan \delta$ of neat PBS and various PBSCNs. For all PBSCNs, the significant enhancement of G' can be seen in the investigated temperature range in compare to that of matrix, indicating OMLS have strong effect on the elastic properties of the neat PBS. Below T_g , there is also strong enhancement of G' for all PBSCNs. In Table 4, we summarized G' values of neat PBS and various PBSCNs at different temperature ranges.

In the temperature range -50 to -10 °C, the increments in G' are 18% for PBSCN1, 31% for PBSCN2, 67% for PBSCN3, and 167% for PBSCN4 compared to that of neat PBS. Furthermore, at room temperature, PBSCN3 and PBSCN4, respectively, show higher incre-

Table 4. Storage Modulus, G' , of Neat PBS and Various PBSCNs at Different Temperature Range

samples	storage modulus, G' /GPa		
	-50 °C	25 °C	100 °C
PBS	1.60	0.26	0.11
PBSCN1	1.88	0.31	0.12
PBSCN2	2.12	0.37	0.15
PBSCN3	2.67	0.47	0.18
PBSCN4	4.27	0.90	0.32
PBSCN5	1.94	0.33	0.13
PBSCN6	3.25	0.60	0.22

ments in G' of 82% and 248% than that of neat PBS, while those of PBSCN1 and PBSCN2 are 18.5% and 44% higher. At 90 °C, only PBSCN4 exhibits a very strong enhancement of G' compared to that of other three PBSCNs.

On the other hand, PBSCNs prepared with qC₁₆-sap clay exhibit relatively weak enhancements in G' as compared to those of PBSCNs prepared with C₁₈-mmt. For PBSCN6, the increments in G' are 102.5% at -50 °C, 128.6% at 25 °C, and 100% at 90 °C than that of neat PBS. However, these values are much less compared to that of PBSCN4 although with comparable clay contents. We expect that two factors are responsible for very high enhancement of modulus in the case of PBSCN4 compared to that of PBSCN6-one is the very high aspect ratio of dispersed clay particles and another factor is the well-ordered intercalated structure in the case of PBSCN4.

The nature of enhancement of G' in PBSCNs with temperature is somewhat different from well-established intercalated (PP-*g*-MA/mmt)²¹ and well-known exfoliated (Nylon-6/mmt)¹ systems. In the later system, there is a maximum of 40–50% increment of G' in comparison to that of the matrix at well below T_g , and above T_g there is a strong enhancement (>200%) in G' . This behavior is common for the nanocomposites reported so far, and the reason is the strong reinforcement effect of the clay particles above T_g when materials become soft.^{12,21} However, in the case of PBSCNs, the order of enhancement of G' is almost the same below and above T_g , and this behavior may be due to the extremely low T_g (-29 °C) of the PBS matrix.

In Figure 5, we summarized the clay content dependence of G' of various PBSCNs obtained under well below T_g (-50 °C). The Einstein coefficient, k_E , derived by using Halpin and Tai's theoretical expression modified by Nielsen, is shown in Figure 5 and represents the aspect ratio (L/D) of dispersed clay particles without intercalation. The Halpin-Tai-Nielsen expression of the modulus of nanocomposites, $G'_{\text{nanocomposite}}$ is given by²²

$$\frac{G'_{\text{nanocomposite}}}{G'_{\text{matrix}}} = \frac{1 + XY\phi_{\text{clay}}}{1 - X\psi\phi_{\text{clay}}} \quad (2)$$

where

$$X = k_E - 1 \quad (3)$$

$$Y = \frac{(G'_{\text{clay}}/G'_{\text{matrix}}) - 1}{(G'_{\text{clay}}/G'_{\text{matrix}}) + X} \quad (4)$$

$$\psi = 1 + \left[\frac{1 - \phi_m}{\phi_m^2} \right] \phi_{\text{clay}} \quad (5)$$

Here G'_{matrix} and G'_{clay} are the storage moduli of the matrix (here PBS) and clay, respectively, X is a constant depending on the type of nanocomposite structure, and it is related to the aspect ratio. ϕ_{clay} and ϕ_m are the volume fraction of clay reinforcement and the maximum packing volume fraction of clay (the value is generally equal to 0.63), respectively. By considering the value of G'_{clay} to be equal to 170 GPa,²³ we have estimated the composition dependence of $G'_{\text{nanocomposite}}/G'_{\text{matrix}}$ according to eqs 2–5, and the values of k_E were estimated by selecting an appropriate value for the best fit to the experimentally obtained $G'_{\text{nanocomposite}}/G'_{\text{matrix}}$ vs ϕ_{clay} plots (Figure 5).

From Figure 5, we can see that PBSCNs (1–3), PBSCN5, and PBSCN6 are well matched with the theoretical curve prepared by considering that k_E equal to 70. So the anisotropy of dispersed intercalated stacked clay particles for these PBSCNs are same (Table 3). On the other hand, PBSCN4 behaves completely different from other PBSCNs, and it is nicely situated in the theoretical curve having a k_E value equal to 160. This observation indicates that the aspect ratio of dispersed clay particles is much higher in the case of PBSCN4 compared to that of other PBSCNs. However, the WAXD analyses (Figure 2 and Table 3) show that the stacking level of PBSCN4 is comparable with that of PBSCN3 that indicates length of the dispersed clay particles is much higher in the case of PBSCN4 compared to other PBSCNs. This is only possible because of strong flocculation of the intercalated silicate layers in PBSCN4.

According to the supplier,¹⁷ they used hexamethylene diisocyanate [OCN-(C₆H₁₂-NCO)] type end groups as the chain extender for the preparation of high molecular weight PBS, and each PBS chain contains one chain extender molecule at the middle, which makes urethane type bonds (see Scheme 2) with terminal hydroxy groups of PBS. That means each high molecular weight PBS chain has two urethane type bonds and these bonds make hydrogen bonds (see Scheme 3) with the silicate hydroxylated edge groups, which leads to the very strong interaction between matrix and silicate layers. This strong interaction is the main driving force for the flocculation of dispersed intercalated silicate layers. One of the most interesting things is that this flocculation tendency of dispersed intercalated silicate layers suddenly increases in PBSCN4 with a clay content of about 3.6 wt % ($\phi_{\text{clay}} = 0.014$, as clearly observed in TEM photographs, Figure 3). For this reason, the aspect ratio of dispersed intercalated silicate layers significantly increased in PBSCN4, and hence mechanical and other material properties (e.g., gas barrier) suddenly jumped from PBSCN3 to PBSCN4.

The same type of behavior in temperature dependence of G' is also observed in the case of PBSCNs prepared with trimethyl octadecylammonium modified mmt (qC₁₈-mmt), where the G' value also suddenly increased with a clay content of 3.6 wt % from a clay content of 2 wt % (Figure 6), and after that there is a systematic increase of modulus with increasing clay content. So, between 2.8 and 3.6 wt % (ϕ_{clay} between 0.011 and 0.014) mmt, a percolation threshold value for strong flocculation exists, and we can control the flocculation of PBSCNs and hence various properties. On the other hand, PBSCN prepared with 3.84 wt % saponite clay does not show such behavior. We expect the clay content in PBSCN6 is lower than the critical value, and this may

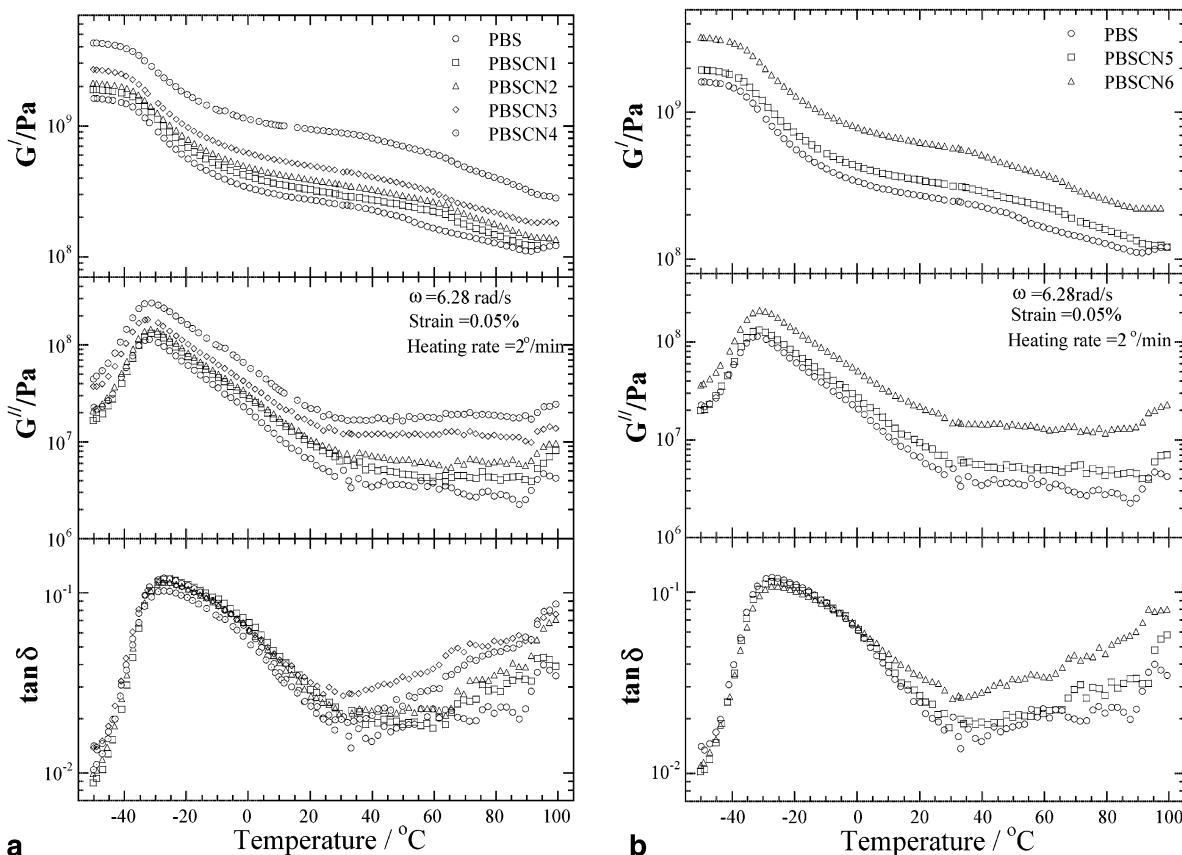


Figure 4. (a) Temperature dependence of the storage modulus (G'), the loss modulus (G'') and their ratio $\tan \delta$ for PBS and various PBSCNs prepared with C_{18} -mmt clay. (b) Temperature dependence of the storage modulus (G'), the loss modulus (G''), and their ratio $\tan \delta$ for PBS and various PBSCNs prepared with qC_{16} -sap clay.

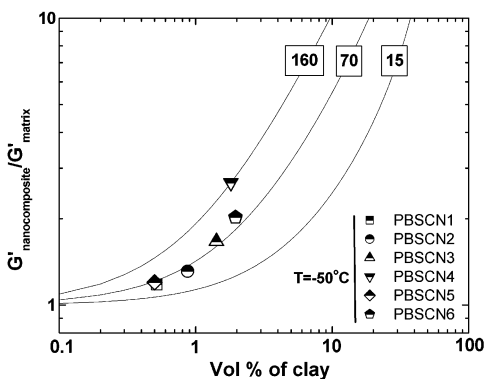


Figure 5. Plots of $G'_{\text{nanocomposite}}/G'_{\text{matrix}}$ vs volume percent of clay for various PBSCNs. The Einstein coefficient, k_E , is shown with the number in the box. The lines show the calculated k_E values from the Halpin and Tai's theory with various k_E values.

be due to much smaller size of saponite clay compared to that of mmt.

We may explain this behavior with the help of classical theory of suspension rheology of conventional filler reinforced systems. According to this theory,²⁴ the rotation of filler in matrix is possible when $\phi_{\text{filler}} < \phi_{\text{critical}} \cong (\text{aspect ratio})^{-1}$. All PBSCNs [$\phi_{\text{clay}} = 0.011 < 0.02 \cong (L_{\text{clay}}/d_{\text{clay}})^{-1}$] studied here follow this relation except PBSCN4 [$\phi_{\text{clay}} = 0.014 > 0.007 \cong (L_{\text{clay}}/d_{\text{clay}})^{-1}$], in which $\phi_{\text{filler}} \gg (\text{aspect ratio})^{-1}$. For this reason in PBSCN4, the rotation of intercalated-and-extended flocculated stacked silicate layers in the matrix is completely hindered, and only translational motion is available. For this reason PBSCN4 behaves like a hard material and hence shows

a very high modulus. This behavior is clearly observed in dynamic storage modulus measurements in the molten state (Figure 7).

The presence of clay particles in the PBS matrix does not lead to a big shift and broadening of the $\tan \delta$ curves of PBSCNs (Figure 4, parts a and b). This behavior may be ascribed to the restricted segmental motions at the organic–inorganic interfaces neighborhood of intercalated PBSCNs.¹² However, a large increment in G'' above T_g becomes clear (Figure 4, parts a and b), indicating the large anisotropy of the dispersed clay particles due to the flocculation enhanced the loss component.

Melt Rheology. The measurement of melt rheological properties of polymer/layered silicate nanocomposites is crucial to gain a fundamental understanding of the processability and structure–property relationship of these materials. Generally, the rheology of polymer melts strongly depends on the temperature at which measurement is carried out. It is well-known that for the thermorheological simplicity, isotherms of storage modulus ($G'(\omega)$), loss modulus ($G''(\omega)$), and complex viscosity ($|\eta^*(\omega)|$) can be superimposed by horizontal shifts along the frequency axis²⁴

$$b_T G'(a_T \omega, T_{\text{ref}}) = b_T G'(\omega, T);$$

$$b_T G''(a_T \omega, T_{\text{ref}}) = b_T G''(\omega, T);$$

$$|\eta^*(a_T \omega, T_{\text{ref}})| = |\eta^*(\omega, T)|$$

where a_T and b_T are the frequency and vertical shift factors respectively, and T_{ref} is the reference temperature. All isotherms measured for pure PBS and for vari-

Scheme 3. Formation of Hydrogen Bonds between PBS and Clay, Which Leads to the Flocculation of the Dispersed Silicate Layers

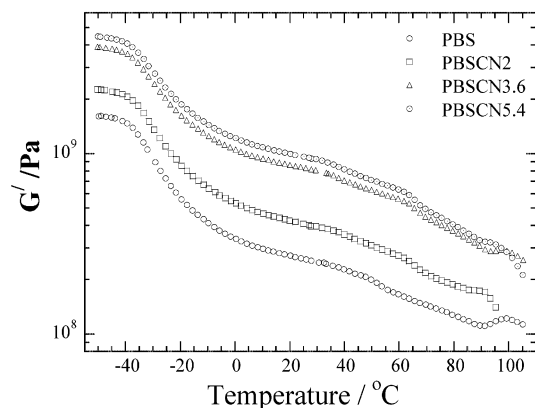
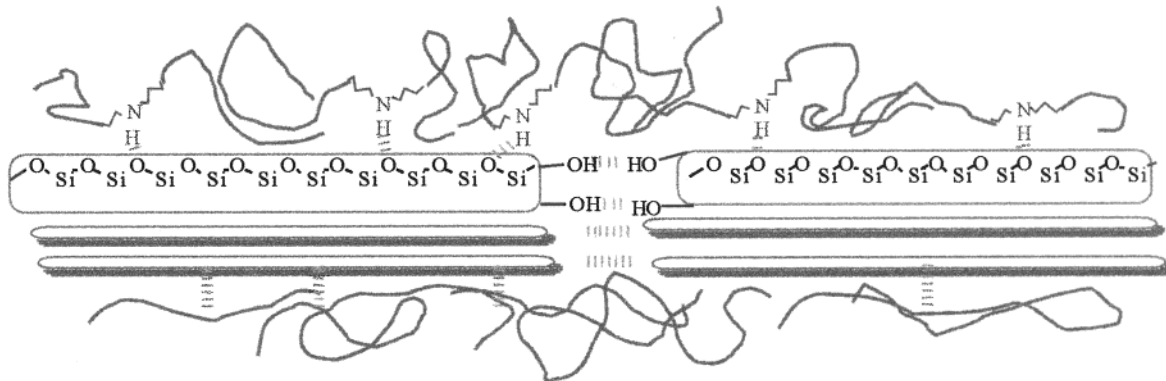


Figure 6. Temperature dependence of storage modulus (G') of PBS and various PBSCNs prepared with qC₁₈-mmt.

ous PBSCNs can be superimposed along the frequency axis.

In the case of polymer samples, it is expected, at the temperatures and frequencies at which the rheological measurements were carried out, that the polymer chains should be fully relaxed and exhibit characteristic homopolymer-like terminal flow behavior; i.e., curves can be expressed by a power-law of $G' \propto \omega^2$ and $G'' \propto \omega$.

The master curves for $G'(\omega)$ and $G''(\omega)$ of neat PBS and various PBSCNs with different wt % of silicate loading are presented in Figure 7, parts a and b. At all frequencies, both $G'(\omega)$ and $G''(\omega)$ for PBSCNs increase monotonically with increasing silicate loading with the exception of PBSCN1 (Figure 7a) and PBSCN5 (Figure 7b) in which viscoelastic responses are almost identical to that obtained for neat PBS. At high frequencies ($a_T\omega > 5$), the viscoelastic behaviors of all PBSCNs are the same, with the exception of only a systematic increase of modulus value with increasing silicate content. On the other hand, at low frequencies ($a_T\omega < 5$), both moduli exhibit weak frequency dependence with increasing clay content, which means that there are gradual changes of behavior from liquidlike [$G' \propto \omega^2$ and $G'' \propto \omega$] to solidlike with increasing clay content.

The terminal regions slope of master curves for $G'(\omega)$ and $G''(\omega)$ are presented in Table 5. The slopes of $G'(\omega)$ and $G''(\omega)$ in the terminal region of the master curves of PBS matrix are 1.8 and 1 respectively, and these values are in the range expected for polydisperse polymers.²⁵ On the other hand, the slopes of $G'(\omega)$ and $G''(\omega)$ are considerably lower for all PBSCNs compared to those of neat PBS with similar molecular weight and

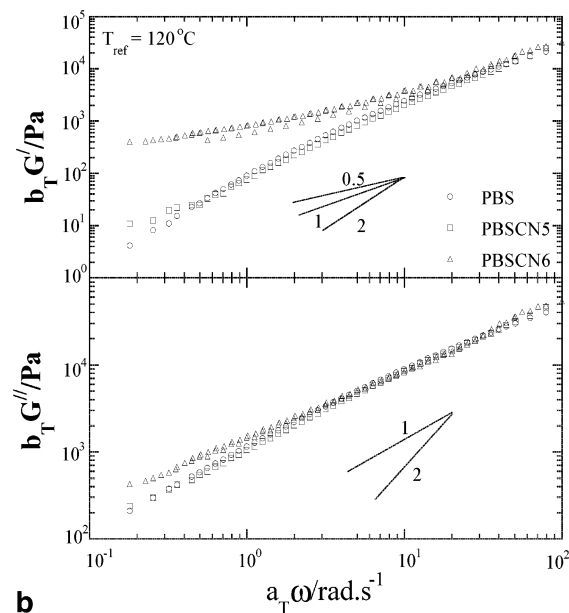
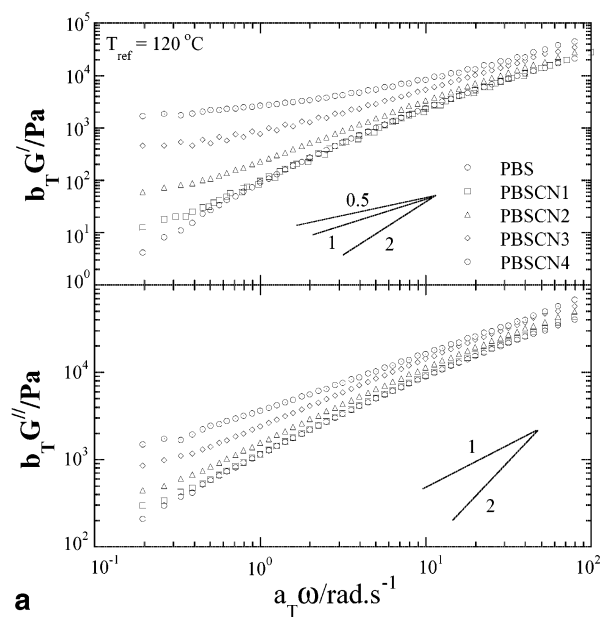


Figure 7. (a) Reduced frequency dependence of the storage modulus, $G'(\omega)$, and the loss modulus, $G''(\omega)$, of PBS and various PBSCNs prepared with C₁₈-mmt clay. $T_{ref} = 120$ °C. (b) Reduced frequency dependence of the storage modulus, $G'(\omega)$, and the loss modulus, $G''(\omega)$, of PBS and various PBSCNs prepared with qC₁₆-sap. $T_{ref} = 120$ °C.

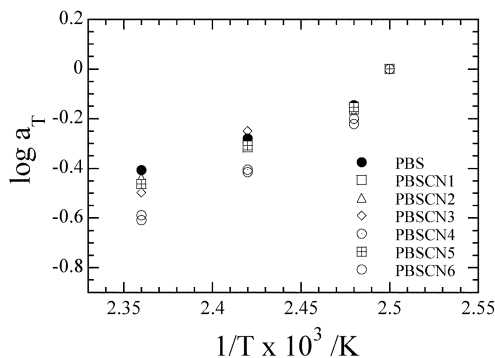


Figure 8. Frequency shift factors of PBS and various PBSCNs (a_T) as a function of temperature.

Table 5. Terminal Region Slopes of $G'(\omega)$ and $G''(\omega)$ vs $a_T\omega$ ($<10 \text{ rad}\cdot\text{s}^{-1}$) for Neat PBS and Various PBSCNs

samples	slope of $G'(\omega)$	slope of $G''(\omega)$
PBS	1.8	1.0
PBSCN1	1.2	0.8
PBSCN2	0.9	0.7
PBSCN3	0.5	0.5
PBSCN4	0.2	0.4
PBSCN5	1.1	0.7
PBSCN6	0.3	0.5

polydispersity. In fact, for PBSCNs with high clay content, $G'(\omega)$ becomes nearly independent at low $a_T\omega$ and exceeds $G''(\omega)$, characteristic of materials exhibiting a pseudo-solidlike behavior.

As seen in Table 3, ξ_{clay} values of PBSCNs are smaller than that of L_{clay} , suggesting the formation of spatially linked structure of the dispersed clay particles in PBS matrix. According to this structure, the individual stacked silicate layers are incapable of freely rotating (only translational motion is available), and hence the relaxation of the structure by imposing small ω is prevented almost completely with high clay content.^{12,26,27} This type of prevented relaxation due to the highly geometric constraints or physical jamming of the stacked silicate layers led to the presence of pseudo-solidlike behavior as observed in the cases of PBSCN4 and PBSCN6, respectively. The formation of this type of spatially linked structure in the PBSCNs with high clay content under molten state is also confirmed by the lower slope values and the higher absolute values of the dynamic moduli in the case of PBSCNs.²⁵

The temperature-dependent frequency shift factor, a_T , used to generate the master curves shown in Figure 7 is shown in Figure 8. The dependence of a_T on the OMLS loading suggests that the temperature-dependent relaxations processes of the PBS melt observed in the viscoelastic measurements are somehow affected by the presence of silicate layers,²⁶ and deviation is significant with high clay content. This behavior is different from so far reported study on polymer/OMLS nanocomposites, which show complete independence of a_T on OMLS loading indicating the temperature-dependent relaxations processes observed in the case of neat polymers under viscoelastic measurements are unaffected by the presence of silicate layers.^{26,27} This behavior may be due to the strong interaction between PBS matrix and OMLS by formation of hydrogen bonds as discussed previously.

The vertical shift factors, b_T , required for the preparation of time-temperature superposition master curves (Figure 7) for neat PBS are in the range 1.05–0.95 and these values changed significantly with OMLS loading

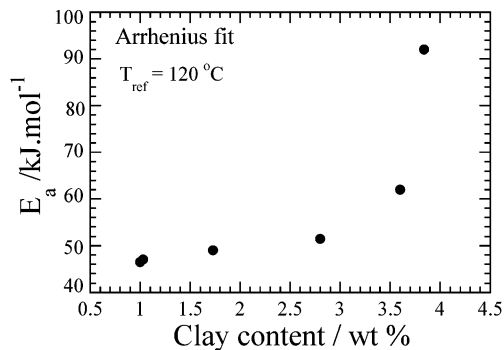


Figure 9. Flow activation energy (E_a) as a function of clay content.

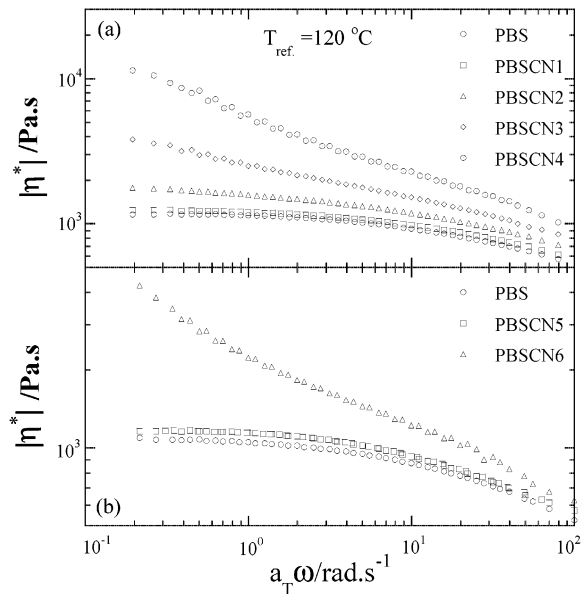


Figure 10. Reduced frequency dependence of complex viscosity ($|\eta^*|(\omega)$) of PBS and (a) PBSCNs prepared with C_{18} -mmt clay and (b) PBSCNs prepared with q C_{16} -sap clay.

(becomes 1.1–0.89 in the case of PBSCNs) and also comparable for all OMLS loading. One possible explanation for this significant fluctuation of b_T values of PBSCNs compare to that of neat PBS may be due to the formation of spatially linked structure in the case of PBSCNs under the molten state with high clay content.

Figure 9 represents the clay content dependent (wt %) flow activation energy (E_a) of neat PBS and various PBSCNs obtained from an Arrhenius fit of master curves. It is clearly observed that E_a value systematically increases with increasing clay content in the case of PBSCNs, which means with high clay content it is very difficult for the materials to flow. This behavior also ascribed the formation of spatially linked structure in PBSCNs to the high clay content under the molten state.

The dynamic complex viscosity [$|\eta^*|(\omega)$] master curves for the neat PBS and various PBSCNs, based on linear dynamic oscillatory shear measurements, are presented in Figure 10. From Figure 10, we can see at low $a_T\omega$ region ($<10 \text{ rad}\cdot\text{s}^{-1}$), neat PBS exhibits almost Newtonian behavior while all PBSCNs (except PBSCN1 and PBSCN5) show very strong shear-thinning tendency. On the other hand, M_w and PDI of neat PBS and various PBSCNs are almost same, thus the high viscosity of PBSCNs can be explained by the flow restrictions of

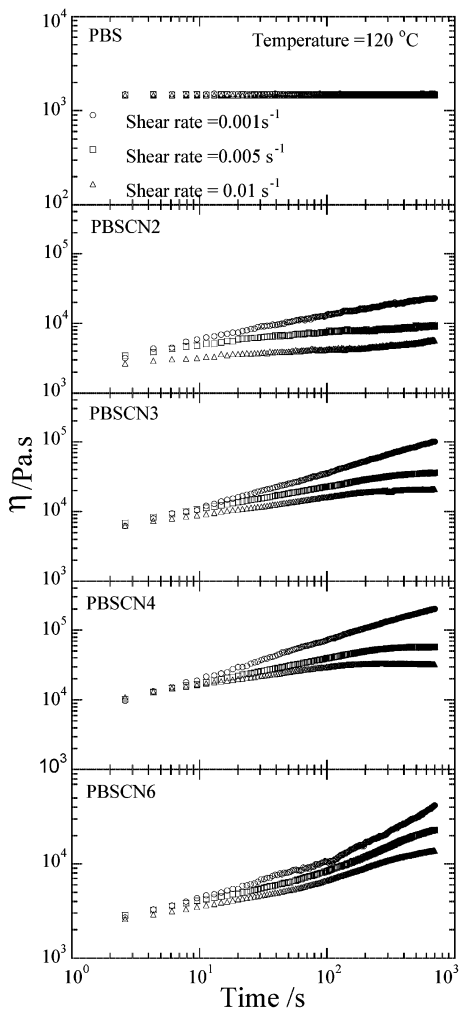


Figure 11. Steady shear viscosity (η) of PBS and various PBSCNs as a function of time.

polymer chains in the molten state due to the presence of clay particles.

We believe this behavior comes from the nature of the clay particles, which are dispersed in the PBS matrix. In our previous study²⁸ on lyophilized smectic clay-toluene suspensions, we observed this type of shear thinning feature of the clay particles in the rapid shear flow. Such a feature is strongly dependent on the shear rate in the dynamic measurements because of the formation of the shear-induced alignment of the dispersed clay particles.²⁹

The steady-shear rheological behavior of neat PBS and a series of intercalated PBSCNs are shown in Figure 11. The steady-shear rheological behavior of PBSCN1 and PBSCN5 are almost identical to that obtained for neat PBS, with the exception of increase viscosity and are not shown in Figure 11. The shear-viscosity of PBSCNs is enhanced considerably at all shear rates with time and at a fixed shear rate increases monotonically with increasing silicate loading. On the other hand, all intercalated PBSCNs exhibit strong rheopexy behavior, and this behavior becomes prominent at low shear rates (0.001 s^{-1}), while neat PBS exhibits a time independent viscosity at all shear rates. With increasing shear rates, the shear-viscosity attains a plateau after a certain time, and the time require to attaining this plateau decreases with increasing shear rates. The possible reason for this type of behavior may

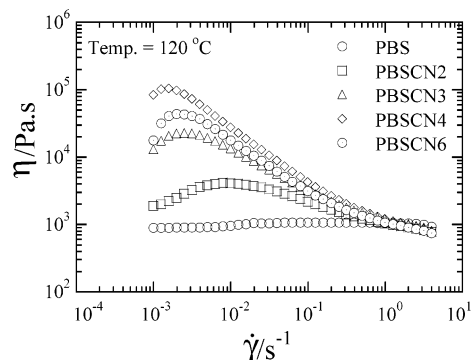


Figure 12. Steady shear viscosity (η) of PBS and various PBSCNs as a function of shear rate.

be due to the planar alignment of the clay particles toward the flow direction under shear. When shear rate is very slow (0.001 s^{-1}), clay particles take a longer time to attain complete planar alignment along the flow direction, and this measurement time (1000 s) is too short to attain such an alignment. For this reason, nanocomposites show strong rheopexy behavior. On the other hand, under high shear rates (0.005 s^{-1} or 0.01 s^{-1}), this measurement time is considerable enough to attain such alignment, and hence, nanocomposites show time-independent shear-viscosity after a certain time.

In Figure 12, we show shear rates dependence of viscosity for neat PBS and various PBSCNs measured at $120 \text{ }^\circ\text{C}$. While the neat PBS exhibits almost Newtonian behavior at all shear rates, whereas PBSCNs exhibited non-Newtonian behavior. At very low shear rates, the shear viscosity of PBSCNs initially exhibits some shear-thickening behavior, and this is corresponding to the rheopexy as observed at very low shear rates (Figure 11). After that, all PBSCNs show a very strong shear-thinning behavior at all measured shear rates and this behavior is analogous to the results obtained in the case of oscillatory shear measurements (Figure 10). Additionally, at very high shear rates, the steady shear viscosities of PBSCNs are comparable to that of neat PBS. These observations suggest that the silicate layers are strongly oriented toward the flow direction at high shear rates, and shear thinning behavior at high shear rates is dominated by that of neat polymer.³⁰

Like the other polymer/OMLS systems,³¹ the data for PBSCNs also exhibit significant deviation from the Cox-Merz relation,³² while neat PBS nicely obeys the empirical Cox-Merz relation, which requires that for the $\dot{\gamma} = \omega$ the viscoelastic data should obey the relationship $\eta(\dot{\gamma}) = |\eta^*(\omega)|$. There are two possible reasons for the deviation of the Cox-Merz relation in the case of nanocomposites: First of all this rule is only applicable for homogeneous systems like homopolymer melts, but nanocomposites are heterogeneous systems. For this reason this relation is nicely obeyed in the case of neat PBS. Second, the structure formation is different when nanocomposites are subjected to dynamic oscillatory shear and steady shear measurements.

Since shear rates dependent viscosity of neat PBS nicely show Newtonian behavior (Figure 12), therefore the Casson relation²⁴ is applicable for PBS. Figure 13a represents the Casson plot for neat PBS and various PBSCNs, and the intercept of this plot give us the stress of these materials at break, i.e., σ_{break} . In Figure 13b, we show the log-log plot of ϕ_{clay} dependence of σ_{break} of various PBSCNs. Up to ϕ_{clay} is equal to 0.011, σ_{break}

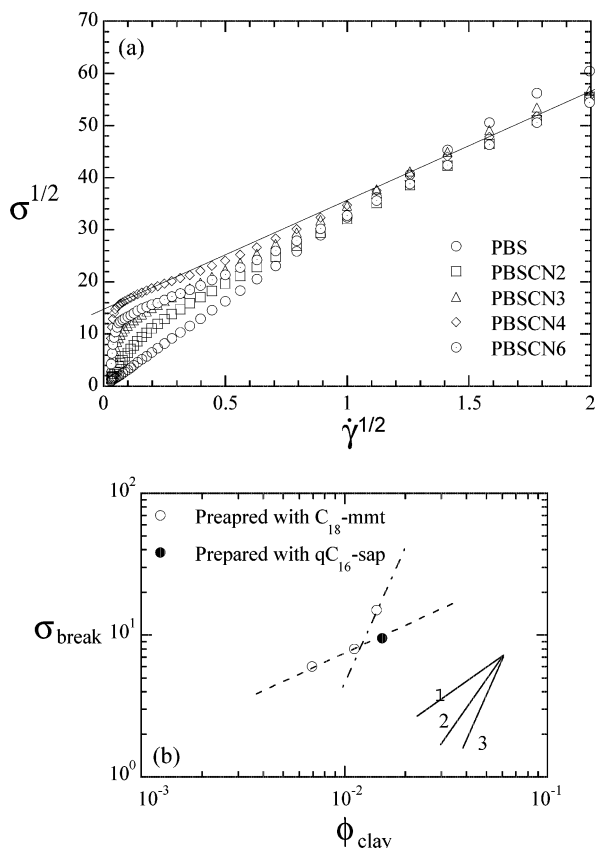


Figure 13. (a) Casson plot of PBS and various PBSCNs. The solid line indicates the intercept of the plot. (b) Clay content dependence of σ_{break} of various PBSCNs.

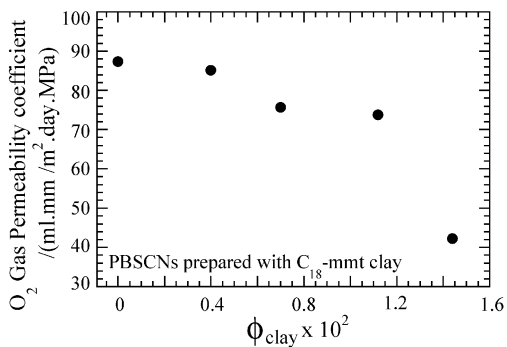


Figure 14. O_2 gas permeability coefficient of various PBSCNs prepared with C_{18} -mmt as a function of clay content.

systematically increases with increasing clay content. On a further increase of clay content, σ_{break} suddenly increases with a very high value of slope 3. This behavior is strongly related to the strong flocculation of the intercalated silicate layers dispersed in PBS matrix, and the value of ϕ_{clay} between 0.011 and 0.014

is the percolation value for such strong flocculation in the case of PBSCNs.

O_2 Gas Permeability Coefficient. Clays are believed to increase the gas barrier properties by creating a maze or “tortuous path” that retard the progress of gas molecules through the matrix resin.^{3,14,15} The O_2 gas permeability coefficients of neat PBS and various PBSCNs prepared with C_{18} -mmt clay are presented in Figure 14. According to the Nielsen model,³³ platelets of length (L_{clay}) and width (D_{clay}) of the clay particles are dispersed parallel in the polymer matrix, and then the tortuosity factor (τ) can be expressed as

$$\tau = 1 + (L_{clay}/2D_{clay})\phi_{clay} \quad (6)$$

where ϕ_{clay} is the volume fraction of the dispersed clay particles. Therefore, the relative permeability coefficient (P_{PBSCN}/P_{PBS}) is given by

$$\frac{P_{PBSCN}}{P_{PBS}} = \frac{1}{1 + (L_{clay}/2D_{clay})\phi_{clay}} \quad (7)$$

where P_{PBSCN} and P_{PBS} are the permeability coefficients of PBSCN and PBS, respectively.

From the above model, it is clear that the gas barrier property of nanocomposites is directly related to the aspect ratio of dispersed clay particles. Figure 14 represents the fact that the gas permeability value of PBSCNs systematically decreased with increasing clay content up to 1.1 vol % (2.8 wt %) and after that there is a sharp decrease in gas permeability with clay content of 1.4 vol % (3.6 wt %). This behavior indicates that the aspect ratio of dispersed clay particles suddenly increased after mmt content of 1.1 vol % and these results again proved that the strong flocculation of dispersed clay particle occurred after mmt content of 1.1 vol % and the percolation value of strong flocculation was situated between the values of mmt of 1.1–1.4 vol %.

Biodegradability. We also investigated the biodegradability of neat PBS before and after nanocomposites preparation with two different kinds of OMLS. In this research we used alkylammonium or alkylphosphonium salts for the modification of pristine layered silicates, and these surfactants are toxic for microorganisms. Lee et al.³⁴ first reported on the biodegradability of aliphatic polyester (BAP) based nanocomposites under compost. They assumed that the retardation of biodegradation of BAP was due to the improvement of the barrier properties of the aliphatic polyester after nanocomposites preparation with OMLS. However, they did not report anything about the permeability. In this paper, we will report some of our very preliminary results on biodegradation of neat PBS and two different nanocomposites under compost at 58 ± 2 °C.

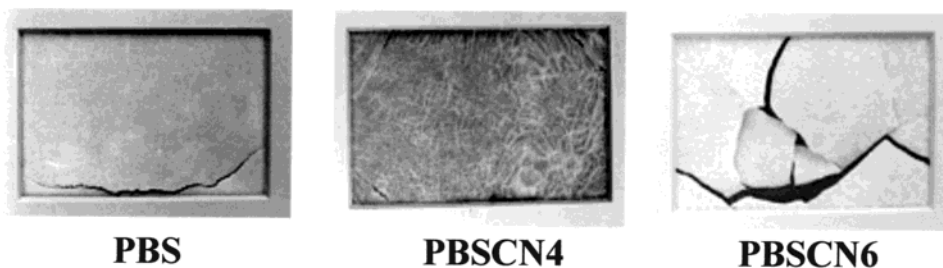


Figure 15. Real pictures of biodegradability of PBS, PBSCN4, and PBSCN6 sheets recovered from compost after 35 days.

Table 6. GPC Results of Various Samples Recovered from Compost after 35 days

samples	$M_w \times 10^{-3}$ (g/mol)	M_w/M_n
PBS	16	2.2
PBSCN4	17	2.3
PBSCN6	15	2.2

Figure 15 shows the real pictures of recovered samples of neat PBS, PBSCN4, and PBSCN6 from compost after 35 days. From the figure, it is clearly observed that many cracks appeared in the nanocomposite samples compared to that of neat PBS. This observation indicates the improved degradability of nanocomposites in compost. This kind of fracture has an advantage for biodegradation because of easy to mix with compost and create much surface area for further attack by microorganisms, and it should be noted here that the extent of fragmentation is directly related to the nature of OMLS used for nanocomposite preparation. We also conducted the GPC measurement of recovered samples from compost, and we found that the extent of molecular weight loss was almost same for all samples (see Table 6). This result indicates that the extent of hydrolysis of PBS in pure state or OMLS filled systems is the same in compost for 35 days.

Therefore, on the basis of compost results and GPC data, we can conclude that the fragmentation tendency of PBS is significantly improved after nanocomposite preparation. At this moment, it is very difficult for us to propose the exact mechanism of compost degradability of PBS because these are very preliminary results, and in our forthcoming report,³⁵ we will try to describe details about the compost degradability of PBS and corresponding nanocomposites.

Conclusions

We have successfully prepared a series of biodegradable PBS/OMLS nanocomposites with two different types of OMLS using a simple melt extrusion. The structure of the nanocomposites is directly related to the nature of the pristine clay and also surfactant used for the modification of clay. The amount of clay content also plays a vital role in controlling the structure of the nanocomposites and, hence, various materials properties. In the case of C₁₈-mmt clay, 1.25 vol % (3.3 wt %) is the percolation threshold value for strong flocculation of the stacked dispersed clay particles in PBSCNs, and for this reason all properties of PBSCNs suddenly changed beyond the percolation value. So we can control the flocculation of dispersed silicate layers in the case of PBSCNs and, therefore, various materials properties.

Acknowledgment. Thanks are due to the Japan Society for the Promotion of Science (JSPS) for the award of a Postdoctoral Fellowship and a research grant to S.S.R. (No. P02152).

References and Notes

- Biswas, M.; Sinha Ray, S. *Adv. Polym. Sci.* **2001**, *155*, 167. Alexander, M.; Dubois, P. *Mater. Sci. Eng. Res.* **2000**, *R28*, 1. Giannelis, E. P.; Krishnamoorti, R.; Manias, E. *Adv. Polym. Sci.* **1999**, *138*, 107. LeBaron, P. C.; Wang, Z.; Pinnavaia, T. *J. Appl. Clay Sci.* **1999**, *15*, 11. Usuki, A.; Kawasumi, M.; Kojima, Y.; Okada, A.; Kurauchi, T.; Kamigaito, O. *J. Mater. Res.* **1993**, *8*, 1174. Kojima, Y.; Usuki, A.; Kawasumi, M.; Okada, A.; Fukushima, Y.; Kurauchi, T.; Kamigaito, O. *J. Mater. Res.* **1993**, *8*, 1185.
- Giannelis, E. P. *Appl. Organomet. Chem.* **1998**, *12*, 675.
- Xu, R.; Manias, E.; Snyder, A. J.; Runt, J. *Macromolecules* **2001**, *34*, 337. Bharadwaj, R. K. *Macromolecules* **2001**, *34*, 9189. Messersmith, P. B.; Giannelis, E. P. *J. Polym. Sci., Part A: Polym. Chem.* **1995**, *33*, 1047. Yano, K.; Usuki, A.; Okada, A.; Kurauchi, T.; Kamigaito, O. *J. Polym. Sci., Part A: Polym. Chem.* **1993**, *31*, 2493. Kojima, Y.; Usuki, A.; Kawasumi, M.; Fukushima, Y.; Okada, A.; Kurauchi, T.; Kamigaito, O. *J. Mater. Res.* **1993**, *8*, 1179.
- Gilman, J. W.; Kashiwagi, T.; Lichtenhan, J. D. *SAMPE J.* **1997**, *33*, 40. Gilman, J. W. *Appl. Clay Sci.* **1999**, *15*, 31. Gilman, J. W.; Jackson, C. L.; Morgan, A. B.; Harris, R. *Chem. Mater.* **2000**, *12*, 1866. Bourbigot, S.; Le Bras, M.; Dabrowski, F.; Gilman, J. W.; Kashiwagi, T. *Fire Mater.* **2000**, *24*, 201. Gilman, J. W.; Jackson, C. L.; Morgan, A. B.; Harris, R., Jr.; Manias, E.; Giannelis, E. P.; Wuthenow, M.; Hilton, D.; Phillips, S. H. *Chem. Mater.* **2000**, *12*, 1866.
- Sinha Ray, S.; Yamada, K.; Okamoto, M.; Ueda, K. *Nano Lett.* **2002**, *2*, 1093. Sinha Ray, S.; Yamada, K.; Okamoto, M.; Ueda, K. *Macromol. Mater. Engg.* **2003**, in press.
- Vaia, R. A.; Jandt, K. D.; Kramer, E. J.; Giannelis, E. P. *Macromolecules* **1995**, *28*, 8080. Krishnamoorti, R. Vaia, R. A.; Giannelis, E. P. *Chem. Mater.* **1996**, *8*, 1728.
- Chen, J. S.; Poliks, M. D.; Ober, C. K.; Zhang, Y.; Wiesner, U.; Giannelis, E. P. *Polymer* **2002**, *43*, 4895.
- Lim, S. T.; Hyun, Y. H.; Choi, H. J.; Jhon, M. S. *Chem. Mater.* **2002**, *14*, 1839. Mani, R.; Bhattacharya, M. *Eur. Polym. J.* **2001**, *37*, 515.
- Narayan, R. Degradation of Polymeric Materials. In *Science and Engineering of Composting: Environmental, Microbiology and Utilization Aspects*; Hoitink, H. A., Keener, H. N., Eds.; OARDC: Wooster, OH, 1993.
- Uesaka, T.; Nakane, K.; Maeda, S.; Ogihara, T.; Ogata, N. *Polymer* **2000**, *41*, 8449 and references therein.
- Fujimaki, T. *Polym. Degrad. Stab.* **1998**, *59*, 209 and references therein.
- Sinha Ray, S.; Maiti, P.; Okamoto, M.; Yamada, K.; Ueda, K. *Macromolecules* **2002**, *35*, 3104. Sinha Ray, S.; Yamada, K.; Okamoto, M.; Ogami, A.; Ueda, K. *Composite Interfaces* **2002**, in press.
- Sinha Ray, S.; Okamoto, K.; Yamada, K.; Okamoto, M. *Nano Lett.* **2002**, *2*, 423.
- Sinha Ray, S.; Yamada, K.; Okamoto, M.; Ogami, A.; Ueda, K. *Macromol. Rapid Commun.* **2002**, *23*, 943. Sinha Ray, S.; Yamada, K.; Okamoto, M.; Ogami, A.; Ueda, K. *Chem. Mater.* **2003**, in press.
- Sinha Ray, S.; Yamada, K.; Okamoto, M.; Ueda, K. *Polymer* **2003**, *44*, 857. Sinha Ray, S.; Yamada, K.; Okamoto, M.; Fujimoto, Y.; Ogami, A.; Ueda, K. *Polymer* **2003**, submitted.
- Sinha Ray, S.; Okamoto, K.; Maiti, P.; Okamoto, M. *J. Nanosci. Nanotech.* **2002**, *2*, 171.
- Yasuda, T.; Takiyama, E. US Pat. 5 391 644, 1995.
- Dritis, V. A.; Tchoubar, C. *X-ray Diffraction by Disordered Lamellar Structures*; Springer-Verlag: New York, 1990; Vol. 99, pp 21–22. Cullity, B. D. *Principles of X-ray diffraction*; Addison-Wesley: Reading, MA, 1978.
- Since the silicate layers are comprised of heavier elements (Al, Si, O) than the interlayer and surrounding matrix (C, H, N, etc.), they appear darker in bright field images.
- Klimentidis, R. E.; Mackinnon, I. D. R. *Clays Clay Mineral.* **1986**, *34*, 155. Grim, R. E. *Clay Mineralogy*; McGraw-Hill: New York, 1953. Pinnavaia, T. J. In *Chemical Physics of Intercalation*; Legrand, A. P., Flandrois, S., Eds.; Plenum: New York, 1987. Güven, N. In *Hydrous Phyllosilicates*; Bailey, S. W., Ed.; Mineralogical Society of America: Washington, DC, 1988; reviews in Mineralogy.
- Nam, P. H.; Maiti, P.; Okamoto, M.; Kotaka, T.; Hasegawa, N.; Usuki, A. *Polymer* **2001**, *42*, 9633. Maiti, P.; Nam, P. H.; Okamoto, M.; Usuki, A.; Hasegawa, N. *Macromolecules* **2002**, *35*, 2042. Kawasumi, M.; Hasegawa, N.; Kato, M.; Usuki, A.; Okada, A. *Macromolecules* **1997**, *30*, 6333.
- Halpin, J. C.; Kardos, J. L. *Polym. Eng. Sci.* **1976**, *16*, 344. Nielsen, L. E. *Mechanical Properties of Polymer and Composites*; New York, Marcel Dekker: New York, 1981; Chapter 7, p 233.
- Somoza, A. M.; Tarazona, P. *J. Chem. Phys.* **1989**, *91*, 517.
- Utracki, L. A. *Polymer Alloys and Blends: Thermodynamics and Rheology*; Hasser Publishers: New York, 1990.
- Hoffmann, B.; Kressler, J.; Stoppelmann, G.; Friedrich, Chr.; Kim, G. M. *Colloid Polym. Sci.* **2000**, *278*, 629. Eckstein, A.; Friedrich, Chr.; Lobbrecht, A.; Spitz, R.; Mulhaupt, R. *Acta*

- Polym.* **1997**, *48*, 41. Friedrich, Chr.; Scheuchenpflug, W.; Neuhausler, S.; Rosch, J. *J. Appl. Polym. Sci.* **1995**, *57*, 499.
- (26) Ren, J.; Silva, A. S.; Krishnamoorti, R. *Macromolecules* **2000**, *33*, 3739. Galgali, G.; Ramesh, C.; Lele, A. *Macromolecules* **2001**, *34*, 852. Solomon, M. J.; Almusallam, A. S.; Seefeldt, K. F.; Somwangthanaroj, A.; Varadan, P. *Macromolecules* **2001**, *34*, 1864.
- (27) Hyun, Y. H.; Lim, S. T.; Choi, H. J.; Jhon, M. S. *Macromolecules* **2001**, *34*, 8084. Choi, H. J.; Cho, M. S.; Kim, J. W.; Kim, C. A.; Jhon, M. S. *Macromol. Rapid Commun.* **2001**, *22*, 320.
- (28) Okamoto, M.; Taguchi, H.; Sato, H.; Kotaka, T.; Tatayama, H. *Langmuir* **2000**, *16*, 4055.
- (29) Okamoto, M.; Nam, P. H.; Maiti, P.; Kotaka, T.; Hasegawa, N.; Usuki, A. *Nano. Lett.* **2001**, *1*, 295. Okamoto, M.; Nam, P. H.; Maiti, P.; Kotaka, T.; Nakayama, T.; Takada, M. Ohshima.; M. Usuki, A.; Hasegawa, N.; Okamoto, H. *Nano. Lett.* **2001**, *1*, 503.
- (30) Krishnamoorti, R.; Giannelis, E. P. *Macromolecules* **1997**, *30*, 4097. Krishnamoorti, R.; Koray, Y. *Curr. Opin. Colloid Interface Sci.* **2001**, *6*, 464.
- (31) Krishnamoorti, R.; Ren, J.; Silva, A. S. *J. Chem. Phys.* **2001**, *114*, 4968.
- (32) Cox, W. P.; Merz, E. H. *J. Polym. Sci.* **1958**, *28*, 619.
- (33) Nielsen, L. *J. Macromol. Sci. Chem.* **1967**, *A1*, 929.
- (34) Lee, S. R.; Park, H. M.; Lim, H.; Kang, T.; Li, X.; Cho, W. J. *Polymer* **2002**, *43*, 2495.
- (35) Sinha Ray, S.; Okamoto, K.; Okamoto, M. Manuscript in preparation.

MA021728Y